PHILOSOPHICAL TRANSACTIONS A

royalsocietypublishing.org/journal/rsta

Research

Cite this article: Bartoli G, Betti M, Marra AM, Monchetti S. 2019 A Bayesian model updating framework for robust seismic fragility analysis of non-isolated historic masonry towers. *Phil. Trans. R. Soc. A* **377**: 20190024.
http://dx.doi.org/10.1098/rsta.2019.0024

Accepted: 26 June 2019

One contribution of 14 to a theme issue 'Environmental loading of heritage structures'.

Subject Areas:
civil engineering, structural engineering

Keywords:
Bayesian framework, model updating, masonry towers, uncertainties quantification, experimental data, fragility curves

Author for correspondence:
Michele Betti
e-mail: mbetti@dicea.unifi.it

THE ROYAL SOCIETY PUBLISHING

A Bayesian model updating framework for robust seismic fragility analysis of non-isolated historic masonry towers

Gianni Bartoli, Michele Betti, Antonino Maria Marra and Silvia Monchetti

Department of Civil and Environmental Engineering, University of Florence, via di S. Marta 3, I-50139 Florence, Italy

GB, 0000-0002-5536-3269; MB, 0000-0002-8389-3355; AMM, 0000-0003-3318-518X; SM, 0000-0001-5775-4311

Seismic assessment of existing masonry structures requires a numerical model able to both reproduce their nonlinear behaviour and account for the different sources of uncertainties; the latter have to be dealt with since the unavoidable lack of knowledge on the input parameters (material properties, geometry, boundary conditions, etc.) has a relevant effect on the reliability of the seismic response provided by the numerical approaches. The steadily increasing necessity of combining different sources of information/knowledge makes the Bayesian approach an appealing technique, not yet fully investigated for historic masonry constructions. In fact, while the Bayesian paradigm is currently employed to solve inverse problems in several sectors of the structural engineering domain, only a few studies pay attention to its effectiveness for parameter identification on historic masonry structures. This study combines a Bayesian framework with probabilistic structural analyses: starting from the Bayesian finite element model updating by using experimental data it provides the definition of robust seismic fragility curves for non-isolated masonry towers. A comparison between this method and the standard deterministic approach illustrates its benefits.

This article is part of the theme issue 'Environmental loading of heritage structures'.

1. Introduction

The European territory, and the Italian Peninsula in particular, is subject to seismic hazard. Recent earthquakes that have hit this territory [1–3] have again highlighted the need for improving the knowledge about the seismic response of historical structures in order to plan proper prevention strategies. The relevance of this problem derives from the significant number of fatalities and injuries caused by masonry structures collapsing during earthquakes, as well as the need to preserve heritage buildings. In this scenario, having even more accurate predictions of the seismic vulnerability of existing masonry structures and providing a quantitative assessment of this accuracy are challenging issues to ensure people's safety.

One of the major concerns when the structural analysis of an existing construction is performed is the unavoidable lack of knowledge in the building process, together with the uncertainties in the parameters governing the structural behaviour: material properties, geometry, boundary conditions, etc. The level of uncertainty connected with these elements needs to be accounted for to accurately assess both the structural safety and the confidence level of the results provided by the analyses. In this respect, the availability of experimental results can provide significant information to calibrate a numerical model of the structure to be employed subsequently to perform seismic analyses [4,5].

In seismic codes, uncertainties involved in the seismic assessment of existing structures are generally treated by simply introducing discrete knowledge levels and associating with each of them a value of the so-called confidence factor. The latter is a reduction factor to be applied to material strength and stiffness, and is supposed to account for all sources of uncertainty involved in the assessment. Despite the simplicity of this approach, several drawbacks are associated with it [6], one of which being the fact that it is unable to correctly account for the additional knowledge that can be acquired by means of the new experimental data [7].

In recent decades, the Bayesian approach has been proven to be an effective theoretical framework for dealing with different sources of uncertainty. The Bayes theorem is commonly employed to derive a posterior probability distribution of a set of uncertain parameters according to both their prior probability distribution (i.e. an initial knowledge about their possible range of values) and the likelihood of the observed data. It allows us to encompass not only the uncertainty quantification with respect to the values of a model parameter but also to account for the acquired additional knowledge. An increased interest has been observed in the use of the Bayesian framework, particularly with reference to the updating of a numerical model from the results of different experimental tests performed on the structure.

However, while the quantification of the role of different sources of uncertainties through the Bayesian approach has been gaining increasing attention in traditional structural engineering fields, e.g. reinforced concrete structures [8,9], only a few studies are reported for masonry structures. Campostrini *et al*. [10] employed a probabilistic methodology based on a Bayesian approach to perform seismic vulnerability assessment at urban scale, which was able to integrate information obtained by rapid survey and take into account the uncertainty and the lack of information on the buildings to be analysed. An overall methodology for evaluating the safety of ancient structures, which employs Bayesian updating techniques, was proposed and applied to a historic aqueduct by Beconcini *et al*. [11]. More recently, Conde *et al*. [12], while investigating the causes that lead to damage in a masonry arch bridge, adopted an inverse analysis procedure based on the Bayesian approach. These studies demonstrate that the Bayesian framework can be employed in the field of historic masonry structures as a useful tool to overcome the difficulties of identifying the proper value for the model parameters when the experimental data are available.

Given this background, this paper proposes a probabilistic Bayesian model updating (BM*u*) framework for robust seismic fragility analyses, with specific reference to the structural typology of non-isolated historic masonry towers. Specific attention has been paid at first to the parameters

involved in the Bayesian procedure in order to define their effect on the obtained posterior distributions. Measurement errors are accounted for by means of a Gaussian distribution centred on the measured values of the experimental data (the natural periods), while modelling uncertainties are taken into account to incorporate the lack of knowledge on the constraint effect originated by the neighbouring structures. The BM*u* framework is subsequently integrated with probabilistic seismic analyses to fully develop the seismic risk assessment path. Robust seismic fragility curves, based on numerical models updated with the dynamic test data, are thus estimated. The concept of robust reliability [13,14] is here introduced considering a set of possible structural models to represent the structure rather than a single model, thus including different sources of uncertainties.

The paper is organized as follows: Section 2 summarizes the main concepts of the methodology proposed to evaluate the robust fragility curve, highlighting the research novelties. Section 3 focuses on the non-isolated masonry tower typology and discusses the relevant sources of uncertainty, which constitute the subject of the Bayesian updating. Section 4 reports the whole procedure employed to obtain robust seismic fragility curves. Eventually, the proposed methodology is compared with an optimization-based deterministic approach to show its effectiveness. Its major benefit is the rigorous treatment of the uncertainties involved in the problem. In fact, while the classical deterministic approach does not allow us to obtain a measure of the uncertainty contained in the model updating procedure, by introducing the Bayesian paradigm, it is possible to obtain a probability distribution of the results and then the possible evaluation of confidence intervals on what has been obtained from the analysis.

2. Methodology

The proposed Bayesian-updated robust fragility curve is derived by calculating the probability of failure of the structure for each considered seismic demand, with the latter expressed in terms of Peak Ground Acceleration (PGA). Other demand measures have been proposed apart from the PGA in literature to characterize the intensity of the seismic hazard, and the interested reader is referred to the study by Casolo [15], where a rational discussion of these measures is presented analysing their correlation with damage indicators; nevertheless, PGA has been chosen in the present study due to its simplicity.

The failure event F is hence defined by using the PGA as an intensity measure of the ground-motion and by evaluating the condition $\mathrm{PGA_c} \leq \mathrm{PGA_d}$ (c stands for capacity and d for demand). The robust probability of failure, denoted by $P_{\bar{D}}(F) = P(F|\bar{D})$, can be written as follows:

$$P_{\bar{D},j}(F) = \int P_j(F \mid \boldsymbol{\theta}) p_{\bar{D}}(\boldsymbol{\theta})\, \mathrm{d}\boldsymbol{\theta} \quad j = 1, \ldots, N, \tag{2.1}$$

where j represents each level of PGA value considered for the definition of the probability of failure, $\boldsymbol{\theta}$ denotes the vector that collects the updated model parameters, $P_j(F \mid \boldsymbol{\theta})$ is the probability of failure for the jth PGA given the parameters $\boldsymbol{\theta}$ and $p_{\bar{D}}(\boldsymbol{\theta})$ represents the updated joint-probability distribution of the model parameters $\boldsymbol{\theta}$. This latter term is obtained as the result of a BM*u*. Based on the Bayes theorem, the prior distribution of the $\boldsymbol{\theta}$ parameters, $p_0(\boldsymbol{\theta})$, is converted into the posterior distribution, $p(\boldsymbol{\theta}|\bar{D})$, by using the experimental data $\bar{D}$ according to the following expression:

$$p_{\bar{D}}(\boldsymbol{\theta}) = p(\boldsymbol{\theta} \mid \bar{D}) = \frac{p(\bar{D} \mid \boldsymbol{\theta}) p_0(\boldsymbol{\theta})}{\int p(\bar{D} \mid \boldsymbol{\theta}) p_0(\boldsymbol{\theta}) d\boldsymbol{\theta}}. \tag{2.2}$$

In equation (2.2), the prior probability density function (PDF), $p_0(\boldsymbol{\theta})$, is built based on the expert judgement and reflects the background information on the uncertain parameters, i.e. before employing the data $\bar{D}$; $p(\bar{D} \mid \boldsymbol{\theta})$ is the likelihood function, that is the probability of obtaining the data $\bar{D}$ given a certain vector of model parameters, $\boldsymbol{\theta}$, while the denominator represents a normalization factor.

Since the BM*u* framework allows us to use different types of information in order to update an initial description of the structural model based on the collected data, the posterior distribution

becomes a measure of the uncertainty of the parameters. They can be once again updated when the additional data become available. The robust fragility curve may be used to identify potentially unsafe scenarios and to promote control strategies when the structure appears vulnerable to possible future severe loads.

This methodology can be summarized as follows:

1. Perform *in situ* tests to collect the relevant experimental data $\bar{D}_k$.
2. Select appropriate numerical models and analysis methods to replicate the seismic behaviour of the structure and the available experimental data.
3. Perform sensitivity analyses to identify the most affecting parameters ($\boldsymbol{\theta}$) of both the seismic behaviour of the structure and the model predictions of the available experimental data.
4. Identify the uncertainties on the $\boldsymbol{\theta}$-parameters.
5. Setting up the BM*u* framework:
    a. Select the prior distribution $p_0(\boldsymbol{\theta})$ through available data and/or expert judgement;
    b. Extract samples from prior distribution and perform the numerical output $\tilde{D}_k(\boldsymbol{\theta})$;
    c. Compute the likelihood function $p(\bar{D} \mid \boldsymbol{\theta})$, taking into account both the modelling and the measurement uncertainties;
    d. Use equation (2.2) to calculate the posterior distribution $p(\boldsymbol{\theta} \mid \bar{D})$;
    e. When the additional experimental data become available, set the posterior distribution as new prior distribution and repeat from point b.
6. Define the conditional probability of failure by taking into account the variability of the uncertain $\boldsymbol{\theta}$-parameters.
7. Use equation (2.1) to integrate the conditional probability of failure on the posterior joint-PDF of the $\boldsymbol{\theta}$-parameters, thus obtaining the robust seismic fragility curve.

The methodology described above is quite general and can be considered as a general framework to be employed and extended to other structural typologies. Next, for illustrative purposes, the methodology is applied for the analysis of a representative historic masonry tower by examining the numerical model, the uncertain parameters and the available experimental data and finally evaluating the seismic fragility curves.

3. Representative masonry tower

The methodology is illustrated on a representative non-isolated historic masonry tower. This structural typology represents the situation where the tower, incorporated within the urban context, interacts in terms of lateral restraint conditions with the surrounding constructions. The adjacent structures, sometimes built in different periods, affect both the dynamic behaviour and the seismic response of the tower, so that distinguishing between isolated and non-isolated towers becomes mandatory [16,17].

As a reference case, one of the towers in the city centre of San Gimignano (Italy) was selected. This tower, the so-called Becci tower, shows a quite regular geometry characterized by a total height of about 38 m and an almost square cross-section sizing 6.8×6.9 m. The thickness of the walls ranges from 2.3 to 1.5 m; the walls are constituted by a multilayered stone masonry typology with the internal and external faces made from a soft stone. The internal core material is unknown for this particular tower, but it may be composed of heterogeneous stone blocks tied by a good mortar, like similar towers in San Gimignano [18]. The section sizes are almost constant along the height of the tower except for the lower level where larger size openings were created to allow the connection of the tower with the adjacent buildings.

The reference case study takes advantage of the availability of experimental dynamic measurements, which allowed us to identify the dynamic behaviour of the tower in terms of modal frequencies [19].

(a) Numerical model

A numerical model of the tower was built and used to replicate the experimental data (as required for the Bayesian finite-element (FE) model updating) and to predict the nonlinear behaviour of the tower under seismic loads.

The numerical model was built by using the FE code ANSYS, while the geometry was based on the results of a geometric survey [20]. A macroelement strategy [21] was employed, and the masonry was modelled as an isotropic continuum: masonry walls were modelled by means of Solid65 elements (eight node isoparametric elements), with a maximum mesh dimension of about 50 cm, paying attention to reproducing the main geometric irregularities in the wall thickness.

While the geometry of the tower is commonly known, the assessment of the interaction between the tower and its confining buildings and the assessment of the material's mechanical parameters deserve more attention since they represent critical issues that may compromise the reliability of the results.

The restraint effect given by the adjacent buildings represents a relevant source of uncertainty because their stiffness is unknown. The scientific literature has proposed reliable approaches for the systematic seismic assessment of masonry towers; however, the proper evaluation of the effects of the interaction between the tower and its confining buildings (when the tower is not an isolated structure) is still an open question [16,17]. From an engineering point of view, this aspect can be accounted for in deterministic approaches by assuming horizontal lateral restraints, either fixed or elastic, whose total height along the tower is usually identified in order to replicate the dynamic behaviour of the tower [22]. In this study, to account for this source of uncertainty, lateral fixed restraints are still assumed, but their height along the tower has been considered as a random variable.

Another source of uncertainty is the assessment of the material properties of the masonry (both linear and strength parameters) constituting the tower walls. Since invasive experimental *in situ* tests are difficult for historic buildings, a preliminary evaluation of the mechanical properties' can be obtained from the classification proposed in the Italian Recommendations [23–25] based on expert judgement or by literature references [26]. These technical documents provide a quantification of the mechanical parameters' variability; document [25], in particular, for the characterization of the masonry properties suggests considering lognormal distributions, thus giving for each masonry typology the standard deviation ($\sigma_{\ln}$) and the mean value corresponding to the associated Gaussian distribution (μ), as reported in table 1.

(b) Masonry modelling

To reproduce the masonry nonlinear behaviour, a smeared crack approach was used, adopting an elastoplastic law with tension cut-off. To achieve this aim, the Drucker–Prager (DP) plasticity model was combined with the Willam–Warnke (WW) concrete failure criterion. This approach has been already extensively used in the scientific literature to model the post-elastic behaviour of the masonry [27–32].

The whole model requires the knowledge of (i) the elastic parameters: E and ν (and ρ); (ii) the plasticity model parameters (DP criterion): c, φ and δ and (iii) the failure criterion parameters (WW criterion): $f_{c,WW}$, $f_{t,WW}$, β_c and β_t.

E denotes the modulus of elasticity and ν denotes the Poisson's coefficient (and ρ represents the mass density). Three additional parameters are required to define the plasticity DP model: the internal friction angle ϕ, the cohesion c and the dilatancy angle δ. The failure criterion is defined by two main parameters: the uniaxial compressive and tensile strengths $f_{c,WW}$ and $f_{t,WW}$. Two additional parameters, the coefficients β_t and β_c, rule the shear stresses on the cracking planes [27,33].

To calibrate these parameters in order to reproduce the brittle cracking behaviour of the masonry in tension, the combination of DP and WW models must comply with the following criteria: (i) the tensile strength $f_{t,WW}$ must be smaller than the tensile strength derived from the

Table 1. Mechanical properties of masonry typologies. f_c, compressive strength; E, elastic modulus; G, shear modulus; ρ, mass density.

masonry typology		f_c (MPa)	E (MPa)	G (MPa)	ρ (kN m^{-3})
irregular stone masonry (pebbles, erratic and irregular stone)	μ	1.40	870	290	19
	$\sigma_{\ln}$	0.29	0.21	0.21	
uncut stone masonry with facing walls of limited thickness and infill core	μ	2.50	1230	410	20
	$\sigma_{\ln}$	0.20	0.17	0.17	
regular stone masonry with good texture	μ	3.20	1740	580	21
	$\sigma_{\ln}$	0.19	0.14	0.14	
soft stone masonry (tuff, limestone, etc.)	μ	1.90	1080	360	16
	$\sigma_{\ln}$	0.27	0.17	0.17	
dressed rectangular stone masonry	μ	7.00	2800	860	22
	$\sigma_{\ln}$	0.14	0.14	0.09	

plasticity model $f_{t,DP}$; (ii) the compressive strength $f_{c,WW}$ must be greater than the compressive strength derived from the plasticity model $f_{c,DP}$ to ensure the correct plastic behaviour of the masonry in the mixed tensile-compression zone [27]. As a result, the proper combination of the plasticity model with the failure criterion allows for an elastic–brittle behaviour of the material in the case of biaxial tensile stresses or biaxial tensile-compressive stresses with a low compression level. On the contrary, the material behaves as elastoplastic in the case of biaxial compressive stresses or biaxial tensile-compressive stresses with a high compression level. Overall, the material behaves as an isotropic medium with plastic deformation and cracking and crushing capabilities. It is noteworthy that the adoption of the elastic perfectly plastic model alone does not allow for reproducing the collapse displacements since the material behaves like an elastoplastic continuum with no limits to deformation.

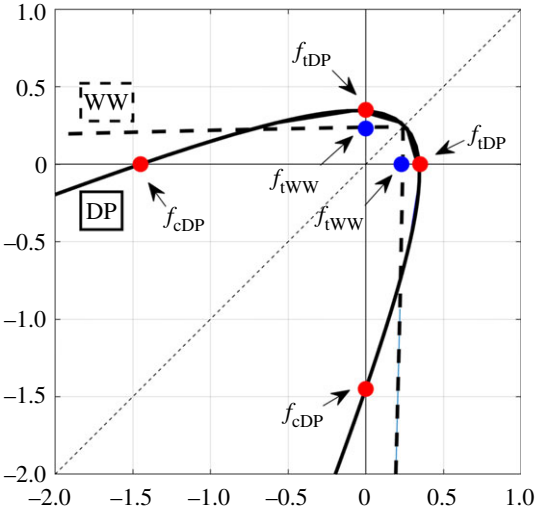

Figure 1. Intersection between the plasticity (DP) and the failure (WW) domains. (Online version in colour.)

Based on the experimental results, Betti *et al.* [27] proposed a calibration procedure between the failure and the plasticity model that allows us to reproduce the experimental tests (both strength and deformability of masonry walls) with good accuracy. The same calibration is used

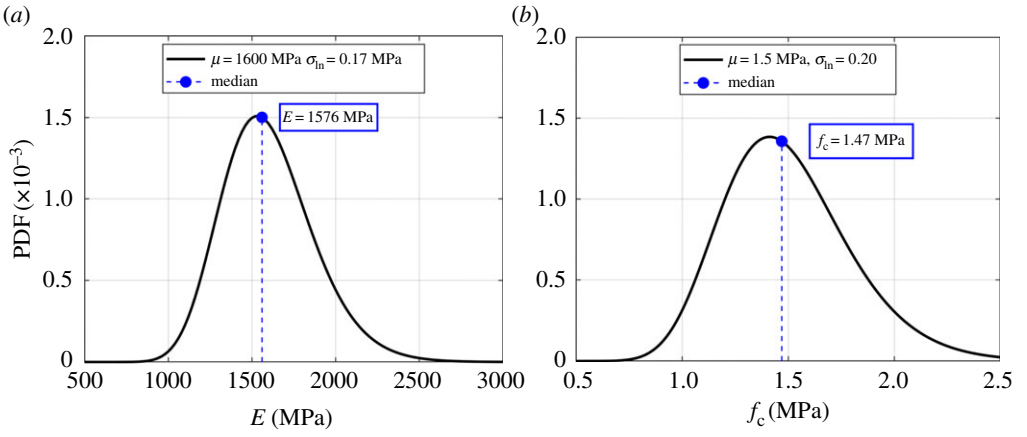

Figure 2. Lognormal PDF of (*a*) the elastic modulus and (*b*) compressive strength of the masonry. (Online version in colour.)

here to define the proper intersection between DP and WW criteria, as shown in figure 1, and the following relation between $f_{t,WW}$ and $f_{c,DP}$ is employed:

$$f_{t,WW} \cong 0.22 f_{c,DP}. \tag{3.1}$$

(c) Uncertainty quantification

The different sources of uncertainties that usually affect the structural assessment of historic structures within a deterministic approach are usually dealt with by simply assuming the most probable values of the chosen parameters. These are selected in a physical variability range by comparing the results of the numerical model with the experimental evidence. However, in order to have a probabilistic characterization of the system, the uncertain parameters can be more properly represented through a PDF.

Next, some possible choices of the PDFs are reported and discussed for the most significant uncertain parameters involved in the seismic vulnerability assessment of the tower.

(i) Mechanical properties of the masonry

Among the mechanical properties of the masonry reported in table 1, the elastic modulus and the compressive and tensile strength play relevant roles in the dynamic identification and seismic behaviour, respectively. Owing to the high level of uncertainty of these mechanical parameters, some PDFs [25] can be selected to represent their variability range. Figure 2 shows the PDFs selected to represent the initial variability range of the elastic modulus (figure 2*a*) and the compressive strength of the masonry (figure 2*b*).

For the elastic modulus, a lognormal PDF has been assumed as characterized by a standard deviation equal to 0.17 MPa and a mean value of the associated Gaussian distribution equal to 1600 MPa. For the compressive strength ($f_{c,DP}$), a lognormal PDF has been employed, characterized by a standard deviation equal to 0.20 MPa, and a mean value of the associated Gaussian distribution, equal to 1.5 MPa; in the following, this variable will be referred to as f_c. Poisson's modulus has been set as a constant and equal to $\nu = 0.2$. These values have been selected taking into account the masonry typology of the considered tower, which can be classified as Soft Stone Masonry [18,24].

(ii) Experimental measurement of the natural periods

Another source of potential uncertainties is due to the experimental results, here represented by the value of the first natural frequencies of the tower (or equivalent to the first natural periods). In

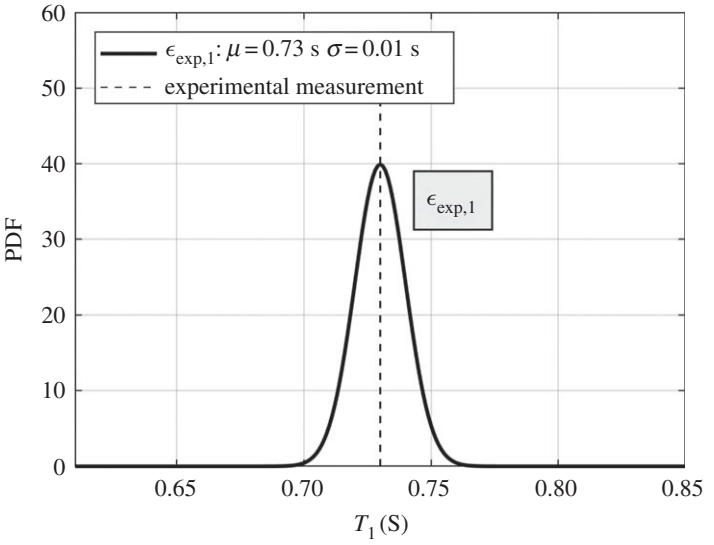

Figure 3. PDF of measurement uncertainties.

Table 2. Experimental measurements of the Becci tower.

tower	direction	natural period, T (s)
Becci	N–S	0.73
	E–W	0.60

the absence of specific information, the uncertainties related to these data have been represented through zero-mean Gaussian distributions, centred on the experimental values. The standard deviation can be assumed as the same for each measurement, but different levels of accuracy can be hypothesized. In this application, only one value of the standard deviation, 0.01 s, was considered, regardless of the considered mode.

The experimental data considered here are the first two natural periods along the two main directions of the structure, as summarized in table 2. Figure 3 shows the PDF of the measurement uncertainties, reporting the distribution of possible values for the first natural period for the Becci tower.

(iii) Lateral restraint condition

Adjacent buildings, as previously discussed, provide a horizontal restraint for the tower, whose effectiveness depends on the stiffness of the surrounding buildings and the effectiveness of the link between them and the tower. This parameter is usually unknown; however, under the assumption that the restraint offered by lateral buildings can be modelled as fixed restraints along a certain portion of the tower with unknown height, the uncertainties related to the lateral restraint condition can be represented through the PDF of the length of the laterally unrestrained part of the tower. By indicating with *effective height* (h) the height of the unrestrained part of the tower [34–36], a schematic representation of this parameter is given in figure 4 for both the main directions of the tower. To account for the uncertainties related to the effectiveness of the restraint conditions introduced by the surrounding structures, a PDF was selected to represent the initial hypotheses about the effective height. In particular, two lognormal PDFs were taken into account to represent the effective height for the North–South direction (N–S) corresponding to the first natural period and for the East–West direction (E–W) corresponding to the second

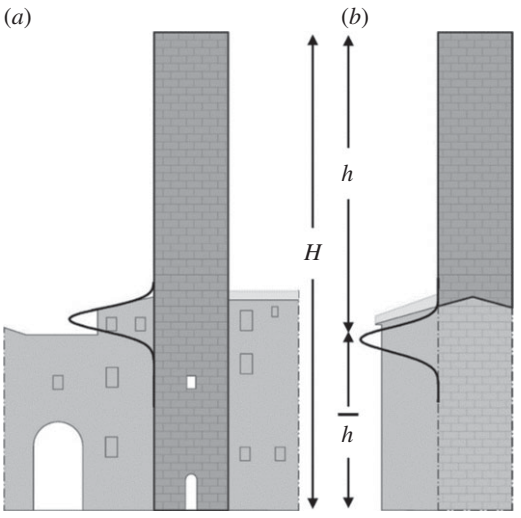

Figure 4. Schematic representation of the effective height (h): PDFs for the E–W (a) and N–S direction (b).

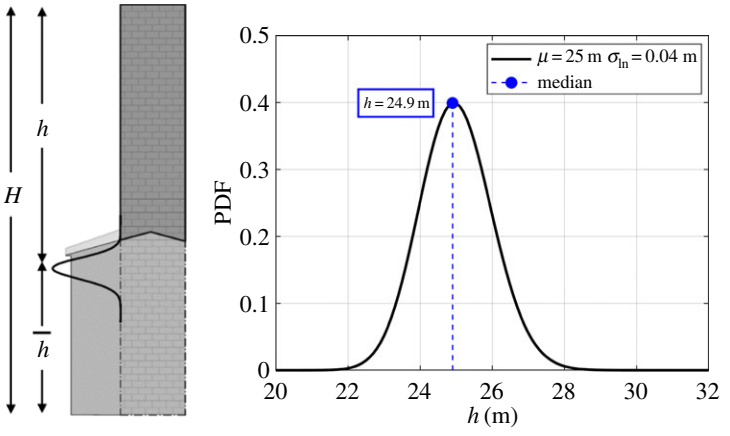

Figure 5. PDF of the effective height of the tower, N–S direction. (Online version in colour.)

natural period, as shown in figure 4. Figure 5 shows the selected lognormal PDF for the N–S direction, characterized by a standard deviation corresponding to 0.04 m and a mean value of the associated Gaussian distribution equal to 25.0 m.

4. Robust seismic fragility curves

The reference case study presented in the previous section is here employed to illustrate the application of the proposed Bayesian methodology to obtain seismic fragility curves. The two terms in the integral of equation (2.1) are here evaluated by showing both the derivation of the BMu and the conditional probability of failure.

(a) Bayesian model updating

The scientific literature has already shown the key role played by the masonry elastic modulus and the effective height in the identification of the dynamic behaviour of non-isolated masonry

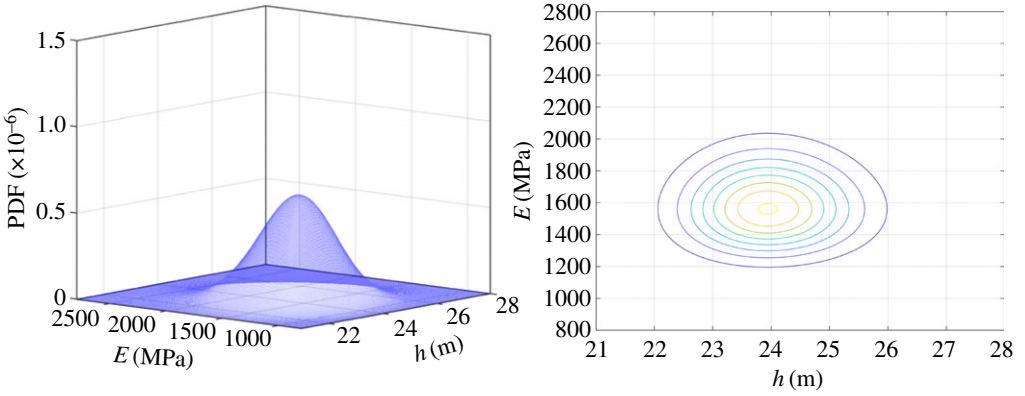

Figure 6. Two views of joint prior-PDF of elastic modulus (E) and effective heigth (h). (Online version in colour.)

towers [34,35]. This suggests, when the experimental data of the natural periods are collected, that the application of the BMu framework can consider the vector $\boldsymbol{\theta}$ as composed by the elastic modulus, E, and the effective height of the tower, h. The Bayesian paradigm is here employed to update the PDF of the component of the vector. The measurement of the first natural period of the tower is used as new information. For the sake of simplicity, it is assumed that the first two bending natural periods are only affected by the restraint conditions along the corresponding mode shape direction. The two selected random variables are hence considered as independent; therefore, their prior joint-PDF can be obtained as the product of the two marginal PDFs, i.e.:

$$p_0(\boldsymbol{\theta}) = p_0(E,h) = p_0(E)p_0(h). \tag{4.1}$$

The assumed marginal distributions for these two random variables are summarized in figure 6.

The application of the Bayes theorem to the BMu framework provides the following relation:

$$p_{\bar{T}}(E,h) = p(E,h \mid \bar{T}) = \frac{p(\bar{T} \mid E,h)p_0(E,h)}{\int\int p(\bar{T} \mid E,h)p_0(E,h)\,\mathrm{d}E\mathrm{d}h}. \tag{4.2}$$

The likelihood function represents the discrepancy between the model output and the measurement, which takes into account two sources of errors: the first is related to the modelling uncertainties and the second is related to the measurement uncertainties. The proposed likelihood function, whose definition is one of the crucial elements in each BMu, has been built considering these two sources of uncertainties:

$$p(\bar{T}|E,h) = \int p(\bar{T}|T,E,h)p_0(T|E,h)\,\mathrm{d}E\,\mathrm{d}h. \tag{4.3}$$

The first term in the integral of equation (4.3) represents the probability of obtaining the natural period $\bar{T}$ given the period T, the elastic modulus E and the effective height h (i.e. the measurement uncertainties), while the second one represents the probability of obtaining T given the elastic modulus E and the effective height h (i.e. the modelling uncertainties). To represent these uncertainties, two zero-mean Gaussian distributions were selected. These distributions are centred on the experimental measurement and the model output, respectively.

By using the experimental measurement of the first natural period, the updated results are illustrated in figures 7 and 8. A reduction is observed in the range of variability of the two random variables (figure 8), together with a significant modification of the shape of the posterior distribution. This change highlights the exclusion of several combinations of the elastic modulus and the effective height. This aspect is particularly evident in figure 7. Indeed, despite the fact that the elastic modulus and the effective height can be considered as independent, these two parameters jointly contributed to the definition of the natural period of the tower. This consideration explains the shape of the posterior joint-PDF, highlighted in figure 7.

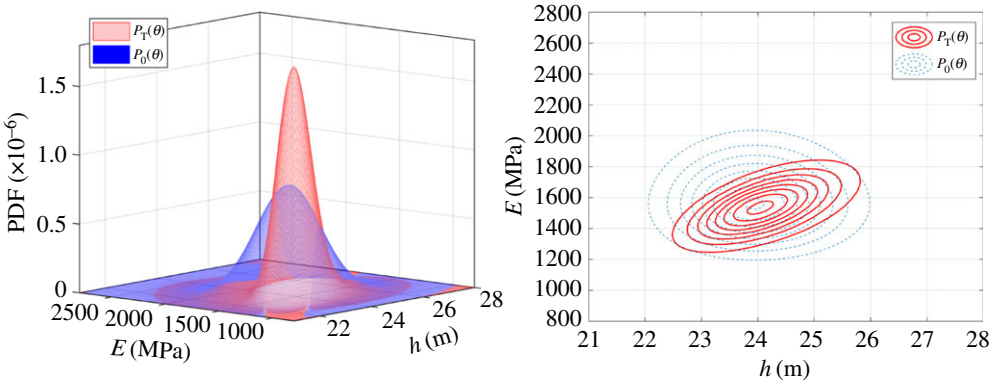

Figure 7. Two views of the prior and posterior joint-PDF of the elastic modulus (E) and the effective height (h). (Online version in colour.)

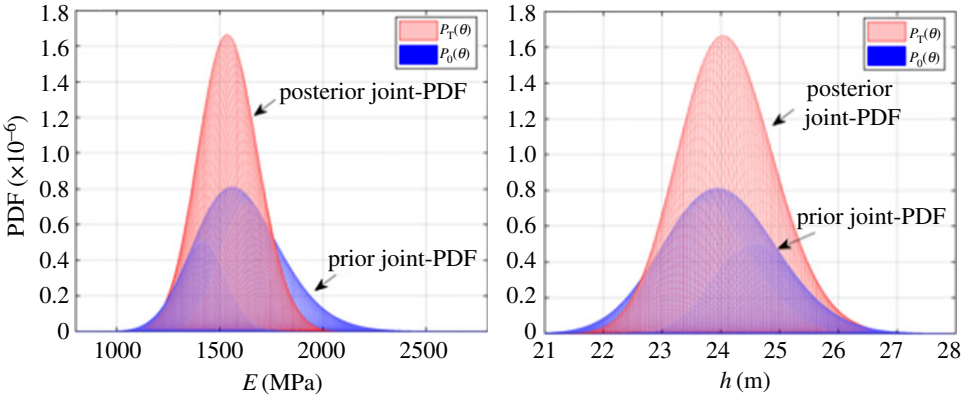

Figure 8. Two lateral views of prior (blue distribution) and posterior (red distribution) joint-PDF of the elastic modulus (E) and the effective height (h). (Online version in colour.)

(b) Conditional probability of failure

The conditional probability of failure is the second element included in equation (2.1) that needs to be evaluated to build the fragility curves. Taking into account the variability of the uncertain parameters of the model, its estimation requires performing a significant number of nonlinear analyses.

(i) Seismic nonlinear analyses

In this work, for illustrative purposes, the seismic vulnerability was evaluated with a pushover approach [37,38]: nonlinear static analyses were carried out by increasing monotonically, under constant gravity loads, a uniform profile of horizontal loads directly proportional to the distribution of the tower mass.

Despite nonlinear time history analyses representing the most sophisticated tool for assessing the seismic vulnerability of a structure, their computational effort is still highly demanding. This drawback is highlighted in several research papers [2,18,39]. The Italian code [23,40], like other international seismic codes, allows us to employ pushover analyses to assess the seismic vulnerability of existing masonry buildings.

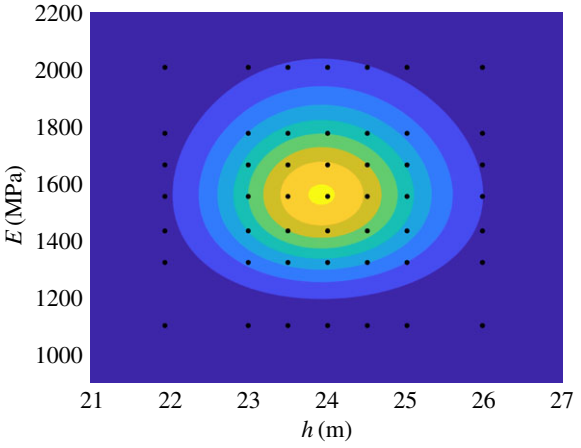

E (MPa)	h (m)
1100	22.0
1325	23.0
1437	23.5
1550	24.0
1662	24.5
1775	25.0
2000	26.0

Figure 9. Posterior joint-PDF of E and h and identification of the samples. (Online version in colour.)

Table 3. Assumed values for the compressive ($f_{c,DP}$) and tensile ($f_{t,WW}$) strength.[a]

no.	c (MPa)	φ (°)	$f_{c,DP}$ (MPa)	$f_{t,DP}$ (MPa)	$f_{c,WW}$ (MPa)	$f_{t,WW}$ (MPa)	β_c (—)	β_t (—)
(1)	0.22	40	0.94	0.28	8.0	0.204	0.75	0.25
(2)	0.27	40	1.16	0.34	8.0	0.251	0.75	0.25
(3)	0.32	40	1.37	0.40	8.0	0.298	0.75	0.25
(4)	0.37	40	1.59	0.47	8.0	0.343	0.75	0.25
(5)	0.42	40	1.80	0.53	8.0	0.387	0.75	0.25

[a]Compressive ($f_{c,DP}$) and tensile ($f_{t,WW}$) strength are connected according to equation (3.1).

The three-dimensional numerical model, after BMu, was employed to evaluate the variability of the seismic behaviour as a function of the variability of the uncertain parameters. The response surface method [41–43] was used to optimize the computational effort by reducing the samples of the input parameters involved in the estimation of the probability of failure $P_j(F|\boldsymbol{\theta})$. It provides a powerful and effective tool for estimating the failure probability, as demonstrated by several applications reported in the scientific literature [43,44]. The method allows us to reduce the computational effort, if compared with classical sampling methods such as Monte Carlo and Latin Hypercube approaches.

Figure 9 reports the selected samples of the elastic modulus of the masonry and of the effective height of the tower. For each combination of these parameters, five pushover analyses were carried out considering the different sets of compressive and tensile strengths reported in table 3. The seismic behaviour of the tower, investigated along the direction corresponding to the first natural period (N–S direction), is summarized in figure 10. The figure summarizes the results of the 245 pushover analyses performed, expressed in terms of capacity curves (i.e. force versus displacement relationships). The capacity curves were built by assuming the base shear and the displacement of the mass centre in the upper section of the tower as a control point.

(ii) Definition of damage states

In order to obtain fragility curves, it is necessary to define limit states (LS) that can be directly checked from the pushover analyses. Usually, for ordinary masonry buildings, three LS are defined [45]: the first corresponds to the exceedance of an elastic behaviour limit (e.g. a reduction of the initial elastic stiffness); the second is reached when the maximum resistance is attained

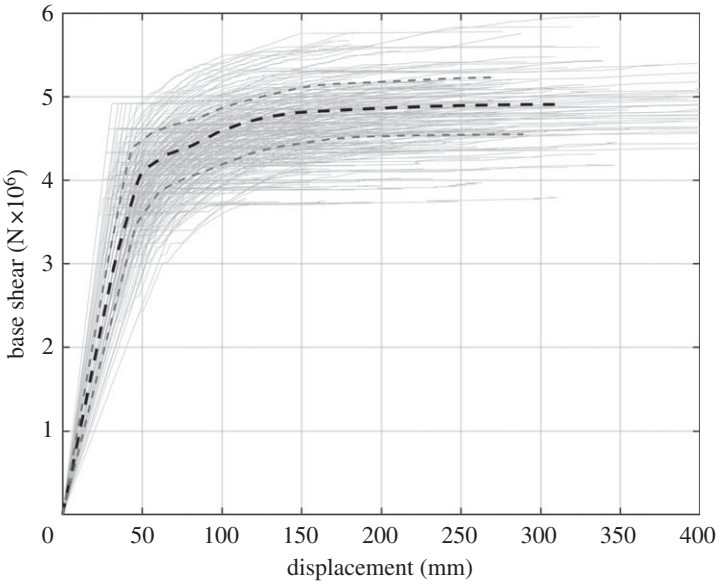

Figure 10. Capacity curves.

and finally the third, the ultimate collapse state, is conventionally identified as a resistance loss corresponding to e.g. 20% of the maximum resistance. In this paper, based on the specific structural typology investigated (i.e. masonry towers), two LS are proposed to build the fragility curves. These two LS are assessed by analysing the current tangent stiffness over the pushover curves and connecting this value with the evolution of the damage on the tower.

In particular, the ratio k/k_{el} between the current tangent stiffness and the initial elastic stiffness on the pushover curve (figure 11*a*) was first evaluated. This ratio is represented in figure 11*b*. It is possible to obtain unambiguous identification of the damage levels by connecting, at each step of the pushover analysis, the ratio k/k_{el} with the cracking pattern on the tower. Based on this procedure, the following two LS were identified:

— Damage limit state (DLS) corresponds to the displacement indicated by δ_{d} (figure 11), where the cracking pattern is widespread, but no masonry elements are crushed; δ_{d} was assumed as the displacement at the level $k/k_{\mathrm{el}} = 5\%$.
— Ultimate limit state (ULS) corresponds to the displacement indicated by δ_{u} (figure 11), where several masonry elements are crushed; in this case, it was assumed as the displacement level at which $k/k_{\mathrm{el}} = 2\%$.

For each LS, the value of the corresponding PGA was obtained through the capacity spectrum method (CSM) [46], expressing the capacity curve and the response spectrum in terms of spectral acceleration and displacement in the acceleration-displacement response spectra format (figure 12).

To underline the effect of different values of compressive strength, figure 12 illustrates the identification of DLS and ULS for one of the analysed cases: $\boldsymbol{\theta} = \{E = 1662\,\mathrm{MPa}, h = 24.0\,\mathrm{m}\}^T$. It is possible to observe that an increase in the compressive strength corresponds to an increase in both displacement and base shear.

A PGA value can be associated with each identified damage level according to CSM (figure 13), and its variability, with reference to the ULS for $\boldsymbol{\theta} = \{E = 1662\mathrm{MPa}, h = 24.0\mathrm{m}\}^T$, is shown in figure 14. The gradual increase in the PGA as a function of f_{c} allows us to introduce a linear approximation (dotted line in figure 14) to assess the PGA level for the compressive strength

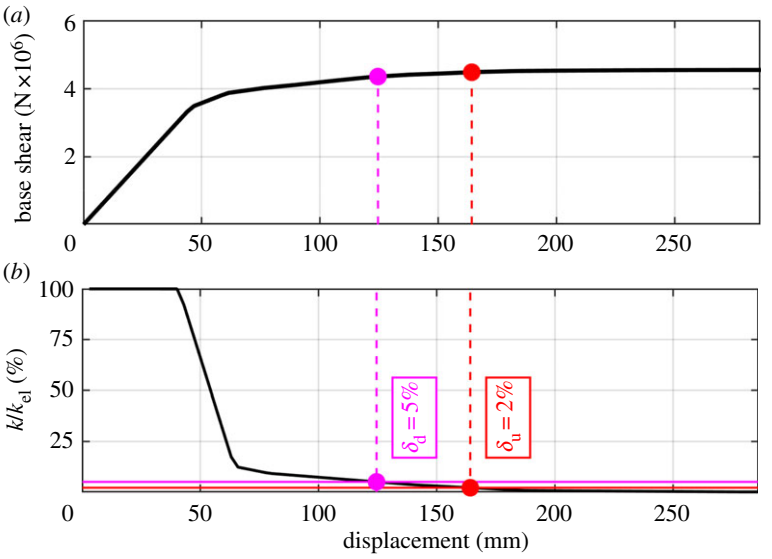

Figure 11. Identification of damage states on a single capacity curve: (*a*) capacity curve and (*b*) stiffness ratio versus displacement. (Online version in colour.)

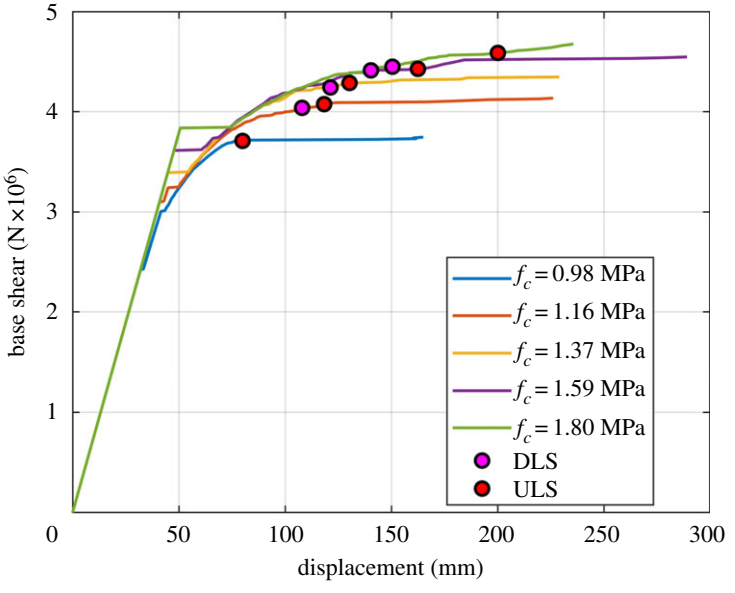

Figure 12. Damage levels (DLS and ULS) on the capacity curves characterized by $\boldsymbol{\theta} = \{E = 1662\ \text{MPa}, h = 24.0\ \text{m}\}^{\mathsf{T}}$. (Online version in colour.)

values not directly analysed. According to [25], a lognormal distribution was subsequently selected (figure 2*b*) to express the uncertainty on f_c. A mean and a standard deviation equal to 1.5 MPa and 0.20 MPa were assumed, respectively. Crude Monte Carlo simulations sampled from the lognormal distribution were carried out. These samples were projected on the linear approximation (response surface), defined in figure 14, thus obtaining for each $\boldsymbol{\theta}_i = \{E_i, h_i\}^T$ the PDF of the PGA. A graphical representation is provided in figure 15*a*. It is noteworthy that this PDF takes into account only the uncertainty on the compressive strength, being referred to a

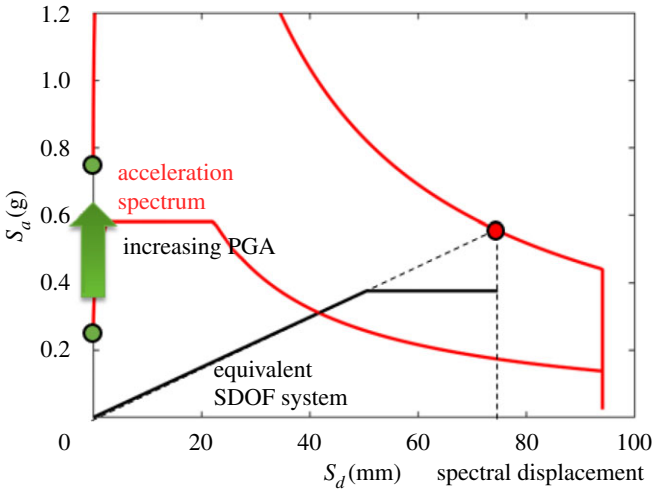

Figure 13. Exemplification of the N2 procedure employed for the assessment of the PGA associated with each damage level. (Online version in colour.)

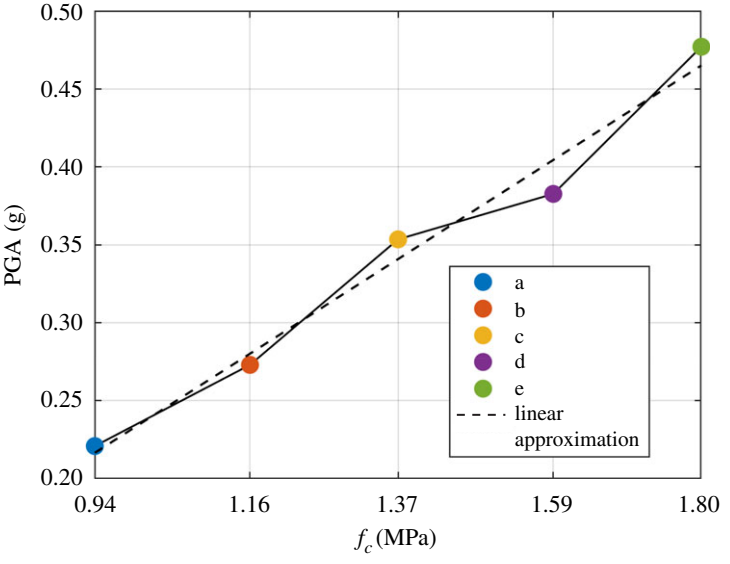

Figure 14. Variability, in terms of compressive strength, of the PGA related to ULS for $\boldsymbol{\theta} = \{E = 1662\ \text{MPa}, h = 24.0\ \text{m}\}^{\mathsf{T}}$ (solid line) and corresponding linear approximation (dotted line); the PDF for the compressive strength is reported in figure 2*b*. (Online version in colour.)

specific $\boldsymbol{\theta}_i$ vector. The probability of failure is then calculated, for different levels of PGA, by integration.

For the sake of clarity, in figure 15*a*, the area under the curve (blue surface), delimitated by a generic PGA level (horizontal red plane), represents the probability of failure. This value is reported in figure 15*b*.

By extending the procedure to all the θ-parameters, it is possible to obtain a surface, on the random variables, $P_j(F|\boldsymbol{\theta})$, which represents the probability of failure conditioned to the θ-parameters and related to the LS.

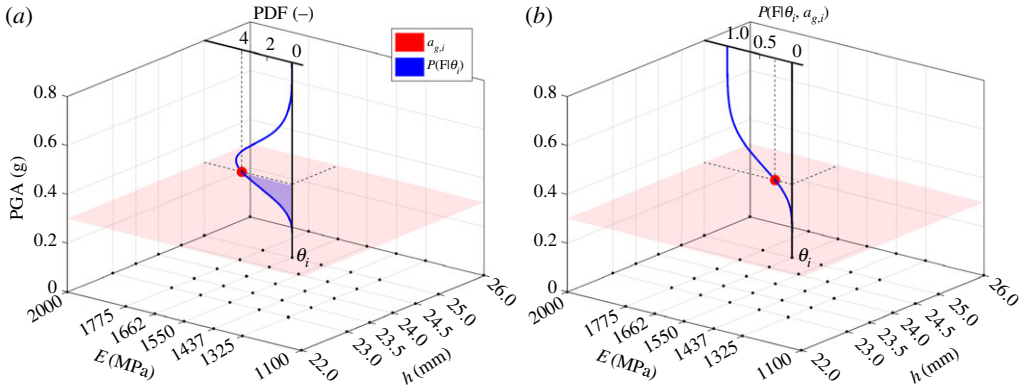

Figure 15. Graphical representation of the probability of failure for a given level of PGA (horizontal plane) and for selected parameters $\boldsymbol{\theta}_i$: (*a*) probability density function and (*b*) failure probability. (Online version in colour.)

(c) Seismic fragility curves

To derive the fragility curve, equation (2.1) is employed. The first term, $P_j(F|\boldsymbol{\theta})$, which represents the probability of failure conditioned to the $\boldsymbol{\theta}$-parameters for the jth level of demand PGA was defined and evaluated in the previous section. The second term, $p_{\tilde{D}}(\boldsymbol{\theta})$, represents the posterior joint-probability distribution of the $\boldsymbol{\theta} = \{E, h\}^T$ random variables vector and is independent from each selected level of PGA.

The fragility curve, which represents the probability of exceedance according to the considered damage levels for each level of PGA, is determined pointwise.

Figure 16 reports the result obtained with the distribution of the compressive strength shown in figure 2*b* combined with the posterior joint-PDF of the $\boldsymbol{\theta}$-vector shown in figure 7. The resulting fragility curve describes the seismic vulnerability, expressed in terms of exceedance probability of the PGA (the considered seismic intensity measure). The proposed methodology allows us to take into account:

— the Bayesian FE-model updating on the $\boldsymbol{\theta} = \{E, h\}^T$ random variables vector, by using experimental dynamic data (i.e. the natural period measurement);
— the variability of the masonry compressive strength, considered as modelling uncertainty on the result of each nonlinear seismic analysis;
— the assumed damage levels.

The proposed methodology combines natural period experimental measurement within the Bayesian framework with modelling uncertainties to derive robust fragility curves.

Usually, in a deterministic framework, the experimental measurements of natural period are employed to build an objective function that measures the error between the experimental values and the ones provided by the numerical model. By changing the values of a selected number of structural parameters, various deterministic linear models can be obtained that meet this objective function. This approach identifies unique values of the selected structural parameters (f.i. boundary condition stiffness, material properties, etc.). Afterwards, some correlations between elastic and inelastic parameters (e.g. between elastic modulus and compressive strength) can be introduced to identify a deterministic nonlinear model. These assumptions lead to a fragility curve without uncertainties (a Heaviside function).

This optimization-based deterministic procedure is compared in figure 17 to the one resulting in this paper; two additional cases are included for illustrative purposes with their corresponding fragility curves evaluated for the damage level ULS.

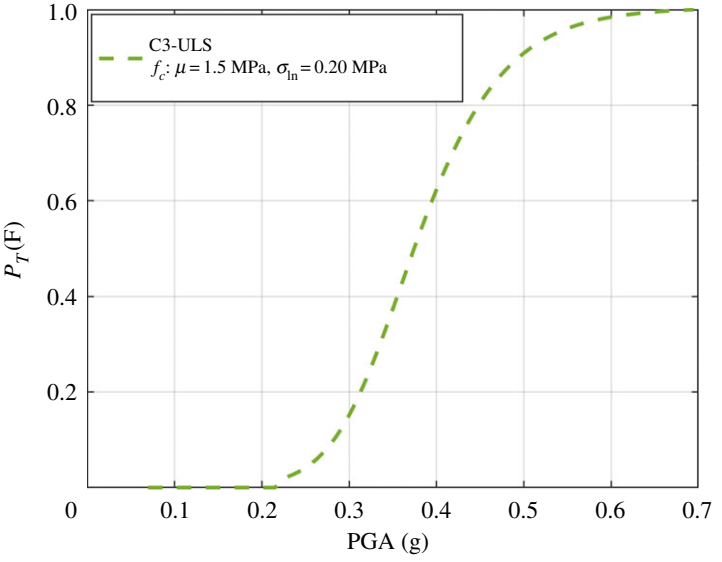

Figure 16. Robust seismic fragility curve (ULS). (Online version in colour.)

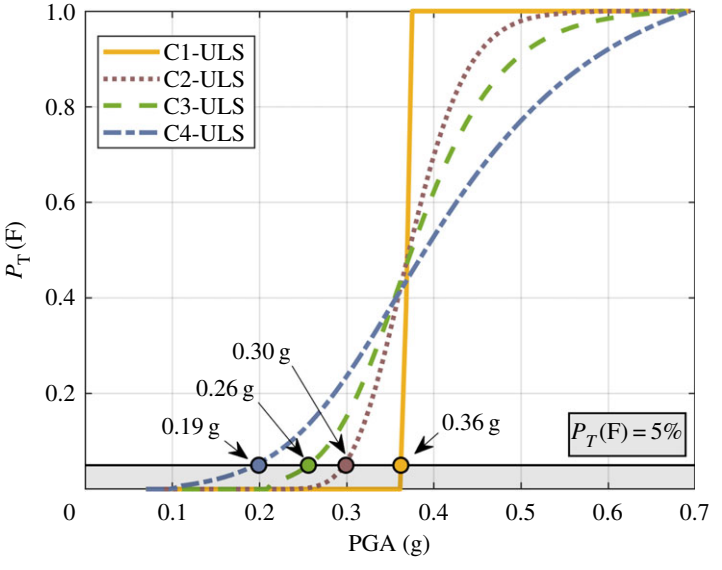

Figure 17. Representation of the effect of different sources of uncertainties in terms of fragility curves. (Online version in colour.)

The continuous yellow line represents the deterministic case, here indicated as *C*1. The reference parameters employed to build the fragility curve are reported in table 4. If no reliable information is available on the inelastic masonry parameters, an additional case (*C*2) can be introduced where, to account for the variability of the compressive strength, a PDF is considered. To this end, a lognormal distribution was selected with the same median value of *C*1 (for comparative purpose); the values are also reported in table 4. This additional case does not account for the Bayesian updating, and its fragility curve is represented with the dotted purple line. The result obtained with the methodology proposed in this paper (denoted as *C*3) is represented with a dashed green line. The natural period experimental measurement is included

Table 4. Characteristics of the reference cases used to evaluate the effect of different sources of uncertainty.

		C1	C2	C3	C4
geometric parameters	external side, a (m)	6.5	6.5	6.5	6.5
	thickness, s (m)	1.5	1.5	1.5	1.5
	total height, H (m)	38.4	38.4	38.4	38.4
	effective height, h (m)	24.9	24.9	$\mu = 24.3$	$\mu = 24.9$
				$\sigma_{\ln} = 0.03$	$\sigma_{\ln} = 0.04$
elastic parameters	specific weight, w (kN m^{-3})	16	16	16	16
	elastic modulus, E (MPa)	1570	1570	$\mu = 1550$	$\mu = 1600$
				$\sigma_{\ln} = 0.1$	$\sigma_{\ln} = 0.17$
plastic parameters	cohesion, c (MPa)	0.34	$\mu = 0.35$	$\mu = 0.35$	$\mu = 0.35$
			$\sigma_{\ln} = 0.2$	$\sigma_{\ln} = 0.2$	$\sigma_{\ln} = 0.2$
	friction angle, φ (°)	40	40	40	40
	compressive strength, f_c (MPa)	1.47	$\mu = 1.5$	$\mu = 1.5$	$\mu = 1.5$
			$\sigma_{\ln} = 0.2$	$\sigma_{\ln} = 0.2$	$\sigma_{\ln} = 0.2$

through the $p_{\tilde{D}}(\boldsymbol{\theta})$, i.e. the posterior joint-PDF of the elastic parameters. The same lognormal distribution considered for the compressive strength in *C*2 was employed to build the term $P_j(F|\boldsymbol{\theta})$. Finally, *C*4, represented by the dash-dotted blue line in figure 17, does not account for the natural period experimental measurement. Its fragility curve was evaluated considering the prior joint-PDF of the elastic parameters ($p_0(\boldsymbol{\theta})$) reported in figure 6. The term $P_j(F|\boldsymbol{\theta})$ accounts for the variability of the compressive strength, and the same lognormal PDF employed for case *C*2 and *C*3 was selected for comparative purposes.

Comparing the C4 fragility curve with others, it is possible to observe that the median collapse value is not maintained. This is due to the fact that the prior joint-PDF of the elastic parameters has a different median value compared with the posterior joint-PDF (figure 7). Moreover, the dispersion of the collapse fragility curves increases from C1 to C4. This variability is a result of the role played by the different sources of uncertainties on the seismic vulnerability of masonry towers, as well as the different approaches employed to define it. Some considerations can be drawn from the seismic vulnerability of the four cases considered, from the observation of the fragility curves reported in figure 17. In terms of PGA, the probability of failure $P_T(F)$ corresponding to the 5th percentile, varies from 0.19 g to 0.36 g for *C*4 and *C*1, respectively. Intermediate PGA levels are obtained in the *C*3 (0.26 g) and *C*2 (0.30 g) cases.

5. Conclusion

A methodology was proposed, which incorporates both modelling and measurement uncertainties into a probabilistic assessment of the seismic vulnerability of non-isolated masonry towers. The procedure allowed us to obtain robust fragility curves, which account for the effect of different sources of uncertainties through a Bayesian updating. In particular, a Bayesian FE-model updating was integrated with probabilistic structural analyses. As experimental datum, the natural period was considered due to its physical relevance for the considered structural typology.

This research was motivated by the need to specifically address the derivation of fragility curves for masonry constructions by incorporating uncertainties into the modelling parameters. The proposed procedure allowed us to include the natural period in the Bayesian updating, hence improving the FE-model prediction in both linear and nonlinear fields. The reported results

are those deriving from nonlinear static analyses of a reference masonry tower, considered as representative of a large number of similar cases. A comparison between this method and the standard deterministic approach illustrates its benefits. In particular: (i) incorporating sources of uncertainties increases the dispersion of the fragility curves; (ii) different approaches employed to incorporate the same sources of uncertainty may originate fragility curves with a significant scattering and (iii) neglecting the effects of uncertainties seems not to be conservative; f.i. if the 5th percentile is considered, the deterministic approach overestimates the collapse PGA value. This, more generally, highlights the need for a proper characterization of the uncertainty parameters (both for linear and nonlinear models), since their propagation in the assessment procedures may largely affect the seismic vulnerability prediction.

This original Bayesian-based framework represents an effective engineering approach, providing an alternative use of the experimental data (short- or long-term field monitoring) to define a probability distribution over a set of plausible structural models. Although the methodology has been illustrated for a specific structural typology, that is the historic masonry towers, the whole procedure may serve as guidance for its application in other structural typologies. The achieved results, in fact, encourage the extension of this approach to the safeguarding of different components of the cultural heritage.

Data accessibility. This article has no additional data.

Authors' contributions. This paper has multiple authors and our individual contributions were as below.

Competing interests. We declare we have no competing interests.

Funding. The present work was partly developed in the framework of the research project MOSCARDO (*ICT technologies for structural monitoring of Ancient Constructions based on wireless sensor networks and drones*) funded by the Tuscany Regional Administration (FAS 2007–2013).

References

1. Augenti N, Parisi F. 2010 Learning from construction failures due to the 2009 L'Aquila, Italy, earthquake. *ASCE's J. Perform. Construct. Facil.* **24**, 536–555. (doi:10.1061/%28ASCE%29CF.1943-5509.0000122)
2. Acito M, Bocciarelli M, Chiesi C, Milani G. 2014 Collapse of the clock tower in Finale Emilia after the May 2012 Emilia Romagna earthquake sequence: numerical insight. *Eng. Struct.* **72**, 70–91. (doi:10.1016/j.engstruct.2014.04.026)
3. Sorrentino L, Cattari S, da Porto F, Magenes G, Penna A. 2018 Seismic behaviour of ordinary masonry buildings during the 2016 central Italy earthquakes. *Bull. Earthquake Eng.* (doi:10.1007/s10518-018-0370-4)
4. Casolo S, Sanjust CA. 2009 Seismic analysis and strengthening design of a masonry monument by a rigid body spring model: the 'Maniace Castle' of Syracuse. *Eng. Struct.* **31**, 1447–1459. (doi:10.1016/j.engstruct.2009.02.030)
5. Diaferio M, Foti D. 2017 Seismic risk assessment of Trani's Cathedral bell tower in Apulia, Italy. *Int. J. Adv. Struct. Eng.* **9**, 259–267. (doi:10.1007/s40091-017-0162-0)
6. Bracchi S, Rota M, Magenes G, Penna A. 2016 Seismic assessment of masonry buildings accounting for limited knowledge on materials by Bayesian updating. *Bull. Earthquake Eng.* **14**, 2273–2297. (doi:10.1007/s10518-016-9905-8)
7. Rota M, Penna A, Magenes G. 2014 A framework for the seismic assessment of masonry buildings taking into account different sources of uncertainty. *Earthquake Eng. Struct. Dynam.* **43**, 1045–1066. (doi:10.1002/eqe.2386)
8. Jalayer F, Iervolino I, Manfredi G. 2010 Structural modeling uncertainties and their influence on seismic assessment of existing RC structures. *Struct. Safety* **32**, 220–228. (doi:10.1016/j.strusafe.2010.02.004)
9. Gardoni P, Der Kiureghian A, Mosalam KM. 2002 Probabilistic capacity models and fragility estimates for reinforced concrete columns based on experimental observations. *ASCE's J. Eng. Mech.* **128**, 1024–1038. (doi:10.1061/(ASCE)0733-9399(2002)128:10(1024))
10. Campostrini GP, Taffarel S, Bettiol G, Valluzzi MR, Da Porto F, Modena C. 2018 A Bayesian approach to rapid seismic vulnerability assessment at urban scale. *Int. J. Architect. Herit.* **12**, 36–46. (doi:10.1080/15583058.2017.1370506)

11. Beconcini ML, Croce P, Marsili F, Muzzi M, Rosso E. 2016 Probabilistic reliability assessment of a heritage structure under horizontal loads. *Probab. Eng. Mech.* **45**, 198–211. (doi:10.1016/j.probengmech.2016.01.001)
12. Conde B, Eguìa P, Stavroulakis GE, Granada E. 2018 Parameter identification for damaged condition investigation on masonry arch bridges using a Bayesian approach. *Eng. Struct.* **172**, 275–285. (doi:10.1016/j.engstruct.2018.06.040)
13. Beck JL, Au SK. 2002 Bayesian updating of structural models and reliability using Markov chain Monte Carlo simulation. *ASCE's J. Eng. Mech.* **128**, 380–391. (doi:10.1061/(ASCE)0733-9399(2002)128:4(380))
14. Papadimitriou C, Beck JL, Katafygiotis LS. 2001 Updating robust reliability using structural test data. *Probab. Eng. Mech.* **16**, 103–113. (doi:10.1016/S0266-8920(00)00012-6)
15. Casolo S. 2001 Significant ground motion parameters for evaluation of the seismic performance of slender masonry towers. *J. Earthquake Eng.* **5**, 187–204 (doi:10.1080/13632460109350391)
16. Castellazzi G, D'Altri AM, De Miranda S, Chiozzi A, Tralli A. 2018 Numerical insights on the seismic behavior of a nonisolated historical masonry tower. *Bull. Earthquake Eng.* **16**, 933–961. (doi:10.1007/s10518-017-0231-6)
17. Bartoli G, Betti M, Galano L, Zini G. 2019 Numerical insights on the seismic risk of confined masonry towers. *Eng. Struct.* **180**, 713–727. (doi:10.1016/j.engstruct.2018.10.001)
18. Bartoli G, Betti M, Monchetti S. 2017 Seismic risk assessment of historic masonry towers: comparison of four case studies. *ASCE's J. Perform. Construct. Facil.* **31**, 04017039. (doi:10.1061/(ASCE)CF.1943-5509.0001039)
19. Pieraccini M. 2017 Extensive measurement campaign using interferometric radar. *ASCE's J. Perform. Construct. Facil.* **31**, 04016113. (doi:10.1061/(ASCE)CF.1943-5509.0000987)
20. Tucci G, Bonora V. 2017. Towers in San Gimignano: metric survey approach. *ASCE's J. Perform. Construct. Facil.* **31**, 04017105. (doi:10.1061/(ASCE)CF.1943-5509.0001085)
21. Lourenço PB. 2002 Computations of historical masonry constructions. *Prog. Struct. Mat. Eng.* **4**, 301–319. (doi:10.1002/pse.120)
22. Bartoli G, Betti M, Giordano S. 2013 In situ static and dynamic investigations on the ''Torre Grossa'' masonry tower. *Eng. Struct.* **52**, 718–733. (doi:10.1016/j.engstruct.2013.01.030)
23. NTC Norme Tecniche per le Costruzioni. 2018 D.M. del ministero delle infrastrutture e dei trasporti del 17/01/2018. Norme tecniche per le costruzioni. p. G.U. 20/02/2018, No. 42 (in Italian).
24. NTC-Instruction. 2019 Circolare n. 7 del 21 gennaio 2019. Istruzioni per l'applicazione dell'Aggiornamento delle 'Norme Tecniche Costruzioni' di cui al Decreto Ministeriale 17 gennaio 2018 (in Italian).
25. CNR Consiglio Nazionale delle Ricerche. 2013 Istruzioni per la valutazione affidabilistica della sicurezza sismica di edifici esistenti. 14/05/2012; 2013 (in Italian).
26. Boschi S, Galano L, Vignoli A. 2019 Mechanical characterisation of Tuscany masonry typologies by in situ tests. *Bull. Earthquake Eng.* **17**, 413–438. (doi:10.1007/s10518-018-0451-4)
27. Betti M, Galano L, Vignoli A. 2016 Finite element modelling for seismic assessment of historic masonry buildings. In *Earthquakes and their impact on society* (ed. S D'Amico), pp. 377–415. Berlin, Germany: Springer Natural Hazards.
28. Cerioni R, Brighenti R, Donida G. 1995 Use of incompatible displacement modes in a finite element model to analyze the dynamic behavior of unreinforced masonry panels. *Comput. Struct.* **57**, 47–57. (doi:10.1016/0045-7949(94)00590-Y)
29. Hejazi M, Moayedian MS, Daei M. 2015 Structural analysis of Persian historical brick masonry minarets. *ASCE's J. Perform. Construct. Facil.* **30**, 04015009. (doi:10.1061/(ASCE)CF.1943-5509.0000746)
30. Korumaz M, Betti M, Conti A, Tucci G, Bartoli G, Bonora V, Korumaz AG, Fiorini L. 2017 An integrated terrestrial laser scanner (TLS), deviation analysis (DA) and finite element (FE) approach for health assessment of historical structures. A minaret case study. *Eng. Struct.* **153**, 224–238. (doi:10.1016/j.engstruct.2017.10.026)
31. Zucchini A, Lourenço PB. 2007 A micro-mechanical model for the homogenisation of masonry. *Int. J. Solids Struct.* **39**, 3233–3255. (doi:10.1016/S0020-7683(02)00230-5)

32. Betti M, Galano L, Petracchi M, Vignoli A. 2015 Diagonal cracking shear strength of unreinforced masonry panels: a correction proposal of the b shape factor. *Bull. Earthquake Eng.* **13**, 3151–3186. (doi:10.1007/s10518-015-9756-8)
33. Willam KJ, Warnke EP. 1975 Constitutive model for the triaxial behaviour of concrete. In Proc. IASBE Seminar on Concrete Structures Subjected to Triaxial Stresses, Bergamo, Italy, 19, 1–30.
34. Bartoli G, Betti M, Marra AM, Monchetti S. 2017 Semiempirical formulations for estimating the main frequency of slender masonry towers. *ASCE's J. Perform. Construct. Facil.* **31**, 04017025. (doi:10.1061/(ASCE)CF.1943-5509.0001017)
35. Diaferio M, Foti D, Potenza F. 2018 Prediction of the fundamental frequencies and modal shapes of historic masonry towers by empirical equations based on experimental data. *Eng. Struct.* **156**, 433–442. (doi:10.1016/j.engstruct.2017.11.061)
36. Bartoli G, Betti M, Marra AM, Monchetti S. 2019 On the role played by the openings on the first frequency of historic masonry towers. *Bull. Earthquake Eng.* (doi:10.1007/s10518-019-00662-9)
37. Pintucchi B, Zani N 2014 Effectiveness of nonlinear static procedures for slender masonry towers. *Bull. Earthquake Eng.* **12**, 2531–2556. (doi:10.1007/s10518-014-9595-z)
38. Marra AM, Salvatori L, Spinelli P, Bartoli G. 2017 Incremental dynamic and nonlinear static analyses for seismic assessment of medieval masonry towers. *J. Perform. Construct. Facil.* **31**, 04017032. (doi:10.1061/(ASCE)CF.1943-5509.0001022)
39. Peña F, Lourenço PB, Mendes N, Oliveira DV. 2010 Numerical models for the seismic assessment of an old masonry tower. *Eng. Struct.* **32**, 1466–1478. (doi:10.1016/j.engstruct.2010.01.027)
40. DPCM. 2011 Direttiva del Presidente del Consiglio dei Ministri per la valutazione e riduzione del rischio sismico del patrimonio culturale con riferimento alle norme techinche per le costruzioni di cui al decreto del Ministero delle infrastrutture e dei trasporti de. 2011. p. G.U. 26/2/2011, No. 47 (In Italian).
41. Isukapalli SS, Roy A, Georgopoulos PG. 1998 Stochastic response surface methods (SRSMs) for uncertainty propagation: application to environmental and biological systems. *Risk Anal.* **18**, 351–363. (doi:10.1111/j.1539-6924.1998.tb01301.x)
42. Youn BD, Choi KK. 2004 A new response surface methodology for reliability-based design optimization. *Comput. Struct.* **82**, 241–256. (doi:10.1016/j.compstruc.2003.09.002)
43. Gupta S, Manohar CS. 2004 An improved response surface method for the determination of failure probability and importance measures. *Struct. Saf.* **26**, 123–139. (doi:10.1016/S0167-4730(03)00021-3)
44. Liel AB, Haselton CB, Deierlein GG, Baker JW. 2009 Incorporating modeling uncertainties in the assessment of seismic collapse risk of buildings. *Struct. Saf.* **31**, 197–211. (doi:10.1016/j.strusafe.2008.06.002)
45. Rota M, Penna A, Magenes G. 2010 A methodology for deriving analytical fragility curves for masonry buildings based on stochastic nonlinear analyses. *Eng. Struct.* **32**, 1312–1323. (doi:10.1016/j.engstruct.2010.01.009)
46. Fajfar P. 1999 Capacity spectrum method based on inelastic demand spectra. *Earthquake Eng. Struct. Dynam.* **28**, 979–993. (doi:10.1002/(SICI)1096-9845(199909)28:9<979::AID-EQE850>3.0.CO;2-1)